Functional Imaging of Localized Prostate Cancer Aggressiveness Using ^{11}C-Acetate PET/CT and ^{1}H-MR Spectroscopy

Ivan Jambor*[1,2], Ronald Borra*[1,3,4], Jukka Kemppainen[3,5], Virva Lepomäki[3,4], Riitta Parkkola[1,3,4], Kirsti Dean[1,4], Kalle Alanen[6], Eveliina Arponen[3], Martti Nurmi[7], Hannu J. Aronen[1,4], and Heikki Minn[3,8]

[1]Department of Diagnostic Radiology, University of Turku, Turku, Finland; [2]2nd Department of Radiology, Comenius University and St. Elisabeth Oncologic Institute, Bratislava, Slovakia; [3]Turku PET Centre, University of Turku, Turku, Finland; [4]Medical Imaging Centre of Southwest Finland, Turku University Hospital, Turku, Finland; [5]Department of Clinical Physiology and Nuclear Medicine, Turku University Hospital, Turku, Finland; [6]Department of Pathology, Turku University Hospital, Turku, Finland; [7]Division of Urology, Department of Surgery, Turku University Hospital, Turku, Finland; and [8]Department of Oncology and Radiotherapy, Turku PET Centre, Turku University Hospital, Turku, Finland

We assessed the ability of ^{11}C-acetate PET/CT, MRI, and proton MR spectroscopy (^{1}H-MRS) to image localized prostate cancer and detect its aggressiveness, using qualitative and quantitative approaches. **Methods:** Twenty-one patients with untreated localized prostate cancer, diagnosed using transrectal ultrasound-guided biopsy, were prospectively enrolled. Cancer laterality was based on the percentage of cancer and the highest Gleason score determined from biopsies. In addition to PET/CT, 3-dimensional ^{1}H-MRS of the entire prostate volume using a quantitative approach was performed. The imaging and histologic findings of 8 patients undergoing subsequent prostatectomy were compared on a sextant level. For each lobe and sextant, standardized uptake values (SUVs) and (choline + creatine + polyamines)–to–citrate (CCP/C) ratios were obtained from ^{11}C-acetate PET/CT and ^{1}H-MRS, respectively. The visual and quantitative findings on PET/CT and MRI data were compared with cancer laterality and aggressiveness based on the Gleason score and with prostate-specific antigen (PSA) velocity and international risk group classification. **Results:** The sensitivity, specificity, and accuracy, on a lobar level using visual analysis, of ^{11}C-acetate PET/CT were 80%, 29%, 71%, respectively, and 89%, 29%, 79%, respectively, using contrast-enhanced MRI. The sensitivity and accuracy of ^{11}C-acetate PET/CT decreased to 64% and 63% and specificity increased to 62% when sextant analysis was performed. The agreement between prostate cancer laterality based on biopsy findings and visual interpretation of ^{11}C-acetate PET/CT and contrast-enhanced MRI was similar at 71%. The mean SUV maximum and CCP/C maximum for the dominant tumor lesion were 5.5 and 1.48, respectively, and did not differ significantly from values in the nondominant lobe. The dominant-lesion SUVs or CCP/C values were not associated with histologically determined prostate cancer aggressiveness, nor did PSA velocity correlate with the SUV or CCP/C values from the entire gland. **Conclusion:** ^{11}C-acetate PET/CT, MRI, and ^{1}H-MRS enable detection of localized prostate cancer with comparable and limited accuracy but fail to provide information on cancer aggressiveness.

Key Words: prostate cancer; ^{11}C-acetate; PET/CT; proton MR spectroscopy

J Nucl Med 2010; 51:1676–1683
DOI: 10.2967/jnumed.110.078667

Prostate cancer is the most common cancer in elderly men and the second leading cause of cancer death in men (*1*). Traditionally, the diagnosis of prostate cancer is based on findings of random transrectal ultrasonography (TRUS)-guided biopsies. Compared with TRUS, MRI has demonstrated a much higher sensitivity for tumor detection but almost the same specificity (*2*), stressing the need for additional metabolic MRI. Proton MR spectroscopy (^{1}H-MRS) has the ability to depict possible cancer in all parts of the gland volume and assist in staging (*3–5*). However, ^{1}H-MRS currently still has several disadvantages such as long acquisition times and the common use of an endorectal coil (*6*). Furthermore, the comparison of published ^{1}H-MRS findings is severely impaired by differences in postprocessing methods, criteria for cancer detection, and predominantly qualitative (visual) interpretation of the data, posing a need for quantitative methods.

PET is a potentially useful tool for prostate cancer imaging. Unfortunately, the most commonly available tracer, ^{18}F-labeled glucose (^{18}F-FDG), has a low sensitivity for cancer detection (*7*). Although preliminary studies have demonstrated that ^{11}C-acetate is a promising tracer for diagnosis of recurrent (*8–10*) or metastatic (*11*) prostate cancer, its use in primary diagnosis is less well established. In particular, the clinical role of ^{11}C-acetate in prostate cancer detection and staging is currently unclear (*12,13*). In vitro studies indicate

Received May 1, 2010; revision accepted Aug. 27, 2010.
For correspondence or reprints contact: Heikki Minn, Department of Oncology and Radiotherapy, Turku PET Centre, Turku University Hospital, Kiinamyllynkatu 4-8, P.O. Box 52, FIN-20521 Turku, Finland.
E-mail: heminn@utu.fi
*Contributed equally to this work.

that ^{11}C-acetate as a marker of enhanced lipid synthesis is appropriate for estimating the growth activity of tumor cells (*14,15*). Hence, we expect ^{11}C-acetate uptake to be higher in those prostate cancers likely to progress clinically than in those that are indolent and should rather be left under active surveillance than treated up front.

Considering that patients with metabolically active prostate cancer are likely to need active treatment, we correlated findings of PET and ^{1}H-MRS with prostate-specific antigen (PSA), clinical risk classification, and pathologic evaluation. Moreover, ^{11}C-acetate PET/CT, ^{1}H-MRS, and MRI were compared for their potential to determine cancer laterality.

MATERIALS AND METHODS

Patients

This was a prospective study of 21 patients (mean age, 63.9 y; age range, 46–78 y) with histologically proven adenocarcinoma of the prostate diagnosed through systematic TRUS-guided biopsies (median, 6 samples per lobe; range, 3–9). Other inclusion criteria were clinical stage T1c–T3aN0 based on TRUS; negative pelvic CT and bone scintigraphy findings; and no previous surgical, radiation, or endocrine treatment for prostate carcinoma. The interval between biopsy and PET was less than 6 mo for 17 patients, less than 1 y (191, 289, and 238 d) for 3 patients, and 779 d for 1 patient (patient 14), whereas the interval between PET and MRI and ^{1}H-MRS ranged from 1 to 21 d, with a mean of 4 d. The study protocol was approved by the Ethics Committee of the Hospital District of Southwest Finland, and each patient gave written informed consent.

Study Design

Patients were first seen by a urologist who was responsible for performing all imaging studies needed to fulfill the inclusion criteria. In addition, standard blood tests were performed, including serum PSA and liver and kidney function tests. All examinations were performed between February 2008 and November 2009.

Patients were divided into prognostic groups according to the following criteria: Gleason score equal to or less than 3 + 3 and equal to or higher than 3 + 4; PSA velocity (calculated from at least 3 measurements of PSA during the past 18 mo) less than 0.4 ng/mL/y, between 0.4 and 1 ng/mL/y, and higher than 1 ng/mL/y; and pretreatment risk groups according to guidelines published by the National Comprehensive Cancer Network (www.nccn.org), as shown in Table 1.

Histopathologic material from random biopsies in all patients and from prostatectomy specimens in 8 patients undergoing surgery after imaging was analyzed by 1 experienced pathologist. The dominant lobe was determined using the combination of the highest number of positive samples, Gleason score, and percentage of cancer tissue in all biopsy samples, with the percentage of cancer given the highest weight if a discrepancy was found among the 3 measures. In prostatectomy specimens, the presence of cancer was defined in 6 regions of interest (ROIs), or sextants, according to the following criteria: the base was defined as the upper third, the mid region was defined as the central third, and the apex was defined as the inferior third, with each third divided between the 2 lobes.

Synthesis of ^{11}C-Acetate

An automated synthesis apparatus was used for the production of ^{11}C-acetate from ^{11}C-carbon dioxide. ^{11}C-acetate was synthesized by reaction of methylmagnesium bromide with ^{11}C-CO_2. Purification was performed using solvent extraction (*16*). The radiochemical yield of ^{11}C-acetate was approximately 4.7 GBq for synthesis, and the obtained radiochemical purity was greater than 99%.

^{11}C-Acetate PET/CT

Patients underwent PET/CT while supine after a 6-h fast and a standard bowel preparation procedure (*17*). PET was performed using a Discovery VCT (GE Healthcare) scanner, with 24 rings of bismuth germanate detectors yielding 47 transverse slices spaced axially by 3.27 mm combined with a helical 64-slice CT scanner. A low-dose CT protocol (120 kV, 30–440 mAs, and 3.75-mm slice thickness) was performed and was also used for transmission correction.

Patients were requested to void 2 h before onset of imaging and then requested to drink 4–5 dL of water to maintain a standardized bladder volume during the study. ^{11}C-acetate tracer (642 ± 78 MBq) was injected in the antecubital vein. A static 240-s emission scan over the pelvic area was acquired 10 min after the tracer injection, followed by 4–5 bed positions covering the torso.

The sinogram data were corrected for dead time, decay, and photon attenuation and reconstructed in a 256 × 256 matrix. Image reconstruction followed a fully 3-dimensional maximum-likelihood ordered-subsets expectation maximum algorithm incorporating random and scatter correction with 2 iterations and 28 subsets. The final in-plane full width at half maximum of the system was 6 mm.

MRI and ^{1}H-MRS Studies

MRI of the prostate was performed using a 1.5-T system (Magnetom Avanto [76 × 18] Q-engine; Siemens). Patients were examined while supine. The body coil was used for excitation, and the appropriate elements of the body-matrix surface coil and spine coil were used for signal reception. High-resolution (0.8 × 0.8 × 3.0 mm) sagittal and transverse T2-weighted turbo spin-echo images were obtained with the following parameters: repetition time (TR)/echo time (TE), 7,430/104 ms; slice thickness, 3 mm; field of view, 200 mm; and matrix size, 256 × 256. Coronal imaging was performed using true fast imaging with steady-state free precession, with a TR/TE of 3.79/1.62, voxel size of 2.0 × 2.0 ×

TABLE 1
Pretreatment Risk Groups Based on Accepted Criteria of National Comprehensive Cancer Network

Risk group	Criteria
Low	Clinical stage T1 or T2a; Gleason score ≤6 and PSA level lower than 10 ng/mL
Intermediate	Clinical stage T2b or T2c; Gleason score of 3 + 4, PSA level of 10–20 ng/mL, or both
High	Clinical stage T3 or higher; Gleason score ≥4 + 3 or PSA level >20 ng/mL

5.0 mm, and matrix size of 256 × 256. T1-weighted contrast-enhanced imaging was performed, with a TR/TE of 635/1.56 ms, flip angle of 10°, voxel size of 1.6 × 1.6 × 5.0 mm, field of view of 300 mm, and matrix size of 192 × 192.

Three-dimensional point-resolved ^{1}H-MRS chemical shift imaging covering the entire prostate region was performed using both lipid and water signal suppression. Outer volume suppression bands were placed around the imaging volume. Automatic and additional manual shimming of the spectroscopic imaging volume were performed. The following chemical shift imaging parameters were used: voxel size, 6.7 × 6.7 × 6.7 mm; TR/TE, 690/120 ms; number of averages, 8; and acquisition time, 14:09 min.

^{11}C-Acetate PET/CT Analysis

The prostate was divided into 2 ROIs covering the right and left lobes. In addition, a sextant approach resulting in 6 ROIs per patient was applied, as explained in the "Study Design" section, in 8 patients receiving prostatectomy. PET data were analyzed quantitatively by calculating maximum and average standardized uptake values (SUVs).

The SUV maximum and average SUV with a 60% threshold (SUV 60%) were measured in all ROIs. SUV maximum and SUV 60% from the dominant lobe (based on histology findings) were correlated with the Gleason score. If pathologic findings from both lobes were equal, then mean SUVs of both lobes were correlated with the Gleason score. ^{11}C-acetate uptake from the entire gland was correlated with PSA, PSA velocity, and the clinical risk group. The rationale for this approach was that all prostatic cells, not just tumor tissue, produce PSA. The laterality of the main lesion (left vs. right) was determined as the lobe with the highest SUV. The quantitative approach was evaluated using receiver-operating-characteristic (ROC) curve analysis. Because of the large overlap between cancer and hyperplasia, we did not use any fixed cutoff value for SUV (*18*). Furthermore, our preliminary ROC analysis did not support a useful cutoff value.

In addition to the quantitative approach, an experienced nuclear medicine physician visually interpreted PET/CT images alone. In visual evaluation, any mono- or multifocal uptake beyond that of periprostatic soft tissue or perirectal fat within the CT-defined prostate gland and detected in more than 1 slice was considered to represent cancer. Diffuse intraprostatic activity or any uptake in the rectum, even if slightly higher than that of the above-mentioned normal tissues, was not classified as cancer.

MRI and ^{1}H-MRS Analysis

An experienced abdominal radiologist analyzed all MR images and was unaware of PET/CT and ^{1}H-MRS results. The suspected presence of cancer on T2-weighted images was defined as a region of low signal intensity in the peripheral zone and as a low-signal-intensity region associated with interruption of the prostate pseudocapsule in the central and transition zones. On dynamic contrast-enhanced T1-weighted images, an early enhancing focus was considered to be tumor tissue.

For analysis of the chemical shift imaging ^{1}H-MRS data, the LCModel software package (version 6.2–1 L, Linux platform) was used (*19*). ^{1}H-MRS data originating from each voxel in the 3-dimensional excited subvolume were processed. The prostate was divided into ROIs and sextants as described in the "Study Design" section.

The individual concentrations of choline, creatine, polyamines, and citrate and the (choline + creatine + polyamines)–to–citrate (CCP/C) (*20*) ratio were represented as numeric values and calculated using the following special spectra control parameter: SPTYPE = "prostate-b." Cramer-Rao minimum variance bounds (%SD) for each individual metabolite and for the CCP/C ratio were determined, in accordance with the LCModel routine output. This numeric built-in quality control allowed us to take into account only those voxels of sufficient quality. For further analysis, only voxels with %SD for choline + creatine + polyamines and citrate of 20% and lower were used, according to the standard LCModel guidelines and manufacturer recommendations. We used the CCP/C ratio because choline, creatine, and polyamines spectral peaks are difficult to separate at 1.5 T (*20*). Patients with no voxels passing our numeric built-in quality control in 1 lobe were excluded. In the same fashion as for ^{11}C-acetate PET/CT, the maximum CCP/C ratio (CCP/C maximum) and average CCP/C ratio (CCP/C average) were correlated with the Gleason score, PSA, PSA velocity, and clinical risk group. The laterality of the main lesion was determined and ROC analysis was performed in a similar fashion as for the ^{11}C-acetate PET/CT data.

Statistical Analysis

All analyses were performed with SAS version 9.1 (SAS Institute, Inc.). SUV maximum from both lobes, SUV 60% from the dominant lobe, and PSA values were log-transformed before statistical analysis because of skewed distributions. The SUVs and CCP/C ratios were compared with Gleason scores using a standard *t* test. PSA velocity and risk groups were treated both as continuous and as categoric variables. The correlations between PSA velocity, risk groups, SUVs, and CCP/C ratios were examined using the Spearman correlation coefficient. Differences between PSA velocity and risk groups' mean scores for both SUV and CCP/C variables were evaluated using 1-way ANOVA. The Pearson correlation coefficient was used to assess the association between log-transformed PSA values, SUVs, and CCP/C ratios. ROC curve analysis was performed for SUVs and CCP/C ratios. A P value of less than 0.05 was considered to be statistically significant.

RESULTS

Clinical Findings

Patient characteristics are shown in Table 2. The mean PSA in our study population was 10.1 ± 6.8 ng/mL (range, 2.9–30 ng/mL). Thirteen patients had a Gleason score of 3 + 3 or less, and 8 patients had a Gleason score of 3 + 4 or more. The numbers of patients belonging to the low-, intermediate-, and high-risk groups were 8, 8, and 5, respectively. The PSA velocity was low (<0.4 ng/mL/y) in 7 patients, intermediate (0.4–1.0 ng/mL/y) in 5, and high (>1.0 ng/mL/y) in 9. In 7 patients (patients 5, 9, 12, 13, 15, 16, and 18), biopsy results suggested unilateral cancer; in 2 patients (patients 3 and 14), pathologic findings from both lobes were equal; and in the remaining 12 patients, the dominant lobe was determined as described in the "Study Design" section. Among the 8 patients who had both biopsy and surgical samples, no discrepancies were found in the laterality of the disease.

Comparison Between Laterality and Imaging

^{11}C-acetate uptake was visualized in the prostate gland in all 21 patients. MRI and ^{1}H-MRS examinations were sim-

TABLE 2
Patient Characteristics

Patient no.	Age (y)	^{11}C-acetate injected activity (MBq)	cTNM	TRUS volume (cm^3)	Gleason score	PSA (ng/mL)	PSA velocity (ng/mL/y)	Clinical risk group
1	61	704	T2cN0	38	4 + 3	5.8	<0.4	High
2	67	599	T1cN0	103	3 + 2	3.9	<0.4	Low
3	52	487	T1cN0	26	3 + 3	3.0	>1.0	Low
4	46	604	T2cN0	17	3 + 4	30.0	>1.0	High
5	67	625	T2aN0	16	2 + 2	2.9	<0.4	Low
6	55	668	T2aN0	45	3 + 3	11.0	>1.0	Intermediate
7	61	704	T2aN0	22	3 + 3	21.0	>1.0	High
8	55	703	T2aN0	32	3 + 4	16.0	>1.0	Intermediate
9	60	736	T1cN0	32	3 + 3	6.0	>1.0	Low
10	78	556	T1cN0	43	3 + 2	9.9	0.4–1.0	Intermediate
11	69	595	T2cN0	19	3 + 3	6.8	<0.4	Low
12	58	663	T1cN0	54	3 + 4	10.0	<0.4	Intermediate
13	63	586	T2aN0	40	2 + 3	8.4	0.4–1.0	Low
14	63	734	T1cN0	30	3 + 3	20.0	>1.0	Intermediate
15	77	599	T1cN0	36	3 + 3	9.8	<0.4	Low
16	64	727	T2aN0	52	2 + 3	10.0	0.4–1.0	Intermediate
17	66	699	T2cN0	21	5 + 4	8.3	>1.0	High
18	77	452	T2aN0	115	2 + 4	7.0	0.4–1.0	Low
19	63	681	T2aN0	50	3 + 2	14.0	<0.4	Intermediate
20	66	691	T2aN0	40	3 + 4	5.9	0.4–1.0	Intermediate
21	73	687	T2cN0	29	4 + 4	3.1	>1.0	High
Mean	63.9	643		41		10.1		
SD	8.27	79		25		6.8		

ilarly performed in all 21 patients. However, ^{1}H-MRS data for patients 2, 18, and 21 and analysis of 18 sextants for patients 1, 3, 4, 5, 6, 7, 8 were excluded from the final MRS analysis because of no voxels in 1 lobe or sextant meeting our described quality requirements. ^{11}C-acetate and ^{1}H-MRS data in the dominant lobe (based on biopsy findings) and in the nondominant lobe are summarized in the supplement table (supplemental materials are available online only at http://jnm.snmjournals.org). The data show that none of the quantitative indices could discriminate between dominant and nondominant lobes, whereas visual evaluation with both PET/CT and MRI was in agreement with the cancer laterality based on biopsy findings in 71% of patients. However, PET/CT and MRI were similarly in agreement in only 71% of patients.

Comparison Between Metabolic Activity and Clinical Aggressiveness

The group with a Gleason score of 3 + 3 or less had a mean CCP/C maximum of 1.38 ± 0.43 and mean CCP/C average of 0.78 ± 0.26. The group with a Gleason score of 3 + 4 or more had mean CCP/C maximum and mean CCP/C average values of 1.70 ± 0.56 and 0.91 ± 0.25, respectively. Despite the observed trend, no statistically significant differences were observed between the mean CCP/C maximum and mean CCP/C average for either group, with P values of 0.20 and 0.33, respectively (Fig. 1A).

The group with a Gleason score of 3 + 3 or less had a mean SUV maximum and mean SUV 60% of 5.7 ± 2.3 and 4.0 ± 1.7, respectively. The group with a Gleason score of 3 + 4 or more had a mean SUV maximum and a mean SUV 60% of

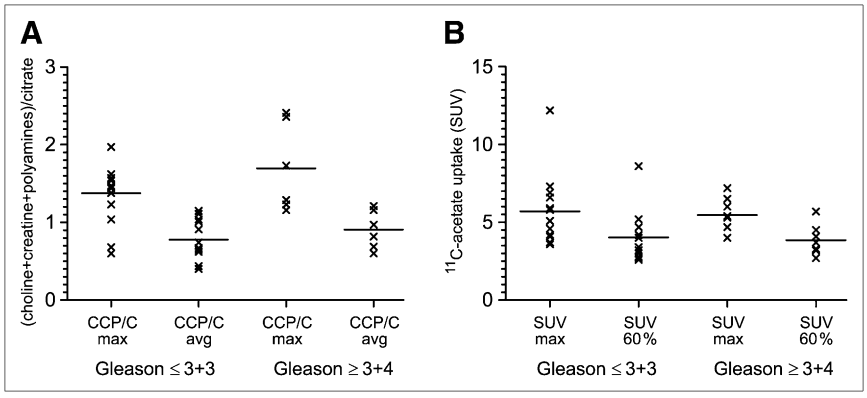

FIGURE 1. Prostate cancer metabolic activity in dominant lobe expressed as CCP/C maximum and CCP/C average on ^{1}H-MRS (A) and SUV maximum and SUV 60% on ^{11}C-acetate PET/CT (B) shows no significant differences between groups with higher and lower Gleason scores. avg = average; max = maximum.

5.5 ± 1.1 and 3.9 ± 0.9, respectively. No statistically significant differences were observed between mean SUV maximum and mean SUV 60% in either the group with a lower Gleason score or the group with a higher Gleason score, with *P* values of 0.97 and 0.98, respectively (Fig. 1B).

^{11}C-acetate uptake and mean CCP/C maximum and mean CCP/C average in all patient groups are summarized in Table 3. SUVs and CCP/C values in patients representing different risk groups and PSA velocity did not differ significantly (Figs. 2 and 3). Likewise, neither SUV nor CCP/C correlated significantly with the baseline serum PSA level.

Diagnostic Accuracy of PET/CT and MRI

Biopsy samples contained cancer in a total of 35 lobes (83%), and only 7 lobes were free of cancer, suggesting, but not confirming, unilateral disease in 7 patients. On the basis of visual analysis of ^{11}C-acetate PET/CT findings, 33 lobes were considered as positive and 9 lobes as negative. Of these, 28 were true-positive and 2 true-negative, yielding a sensitivity, specificity, and accuracy of 80%, 29%, and 71%, respectively, for ^{11}C-acetate PET/CT on a lobar basis. Visual analysis of MR images revealed 36 positive and 6 negative lobes, of which 31 were true-positive and 2 true-negative. Visual analysis resulted in a sensitivity, specificity, and accuracy of 89%, 29%, and 79%, respectively.

The visual analysis of ^{11}C-acetate PET/CT on a sextant level was more specific but less sensitive than based on biopsy evaluation. From a total of 48 sextants at pathologic analysis, 22 (46%) were positive for cancer and 26 were negative. On ^{11}C-acetate PET/CT, 24 sextants were positive and 24 negative, with 14 true-positive and 16 true-negative, respectively. This resulted in sensitivity, specificity, and accuracy of 64%, 62%, and 63%, respectively, for PET/CT. On the basis of visual analysis of MRI data, 20 sextants were considered positive and 28 sextants negative, of which 12 were true-positive and 18 true-negative. These numbers resulted in a sensitivity, specificity, and accuracy of 55%, 69%, and 63%, respectively.

DISCUSSION

The current study is the first, to our knowledge, to prospectively assess the accuracy and applicability of ^{11}C-acetate PET/CT for the detection of aggressiveness of localized prostate cancer in patients whose diagnosis is based mainly on biopsy after PSA screening in an asymptomatic phase. It has been suggested that the dominant lobe (containing the index lesion) determines the aggressiveness of the disease (*21*). For newer radiotherapy techniques such as high-dose-rate brachytherapy or biologically guided radiotherapy, determining the dominant lobe would be of utmost importance. Therefore, it is of clinical importance to study whether imaging helps find this dominant (index) lesion.

We found that ^{11}C-acetate PET/CT—although providing a reasonable clinical tool for visual detection of prostate cancer in our patient population with localized disease—did not provide information on cancer aggressiveness. The inability of ^{11}C-acetate PET to detect prostate cancer aggressiveness may be explained by increased uptake in noncancerous tissue such as hyperplastic and inflamed tissue. Kato et al. (*18*) were the first to report no statistical difference in ^{11}C-acetate SUVs between prostate cancer and benign prostatic hyperplasia. However, their initial study consisted only of 6 patients with histologically confirmed prostate cancer.

The first study suggesting the value of ^{11}C-acetate in prostate cancer imaging (*22*) showed that ^{11}C-acetate had higher sensitivity than ^{18}F-FDG in primary tumor evaluation. When we combined our findings with data from Oyama et al. (*22*) and Kato et al. (*18*), we concluded that individual measurements of SUV on ^{11}C-acetate PET or PET/CT, especially for a low likelihood of cancer, are not useful for primary diagnosis. However, our finding does not necessarily rule out metabolic imaging with ^{11}C-acetate in the setting of staging (*17*).

In the literature, there currently is no consensus about the use of ^{1}H-MRS for prostate cancer detection (*3–5*). We quantitatively analyzed all voxels containing prostatic tissue, eliminating the investigator-dependent variations. In addition, a standardized quality control rule was used for the fit of each individual spectrum. Three patients were excluded from the ^{1}H-MRS analysis because of the low quality of the obtained spectra. In the current study, we chose to select relevant and high-quality ^{1}H-MRS spectra for correlation with ^{11}C-acetate and pathologic findings by including only data with a %SD for choline + creatine + polyamines and citrate of 20% or lower, in contrast to other studies that selected data on the basis of signal-to-noise ratio alone (*23*). The rationale for our choice was 2-fold: the selection based on %SD could be automated for each

TABLE 3
Relationship Between Pretreatment Prognostic Factors, ^{11}C-Acetate PET/CT, and ^{1}H-MRS

	PSA velocity (ng/mL/y)			Clinical risk group		
Prognostic factor	<0.4	0.4–1.0	>1.0	1	2	3
SUV maximum	5.6 ± 1.3	6.6 ± 3.2	5.6 ± 1.2	5.1 ± 1.1	6.4 ± 2.7	6.1 ± 1.1
SUV 60%	3.6 ± 0.8	3.9 ± 1.2	3.6 ± 0.7	3.3 ± 0.6	4.0 ± 1.0	3.9 ± 0.7
CCP/C maximum	1.52 ± 0.48	1.37 ± 0.10	1.72 ± 0.41	1.41 ± 0.32	1.77 ± 0.43	1.43 ± 0.37
CCP/C average	0.70 ± 0.09	0.76 ± 0.20	0.88 ± 0.27	0.73 ± 0.22	0.85 ± 0.22	0.78 ± 0.23

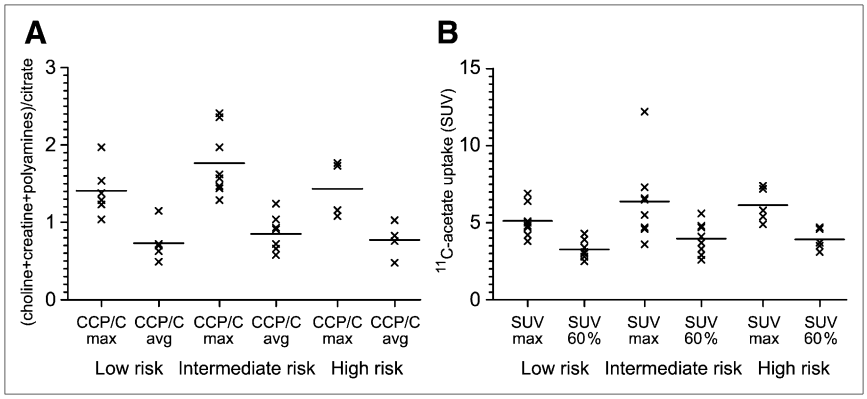

FIGURE 2. Quantitative ^{1}H-MRS (A) and ^{11}C acetate PET/CT (B) show no significant difference between pretreatment risk groups. avg = average; max = maximum.

metabolite in each individual voxel using the LCModel table output, thus avoiding human error, and we found that in our current dataset this method best excluded outlier values resulting in unrealistically high (*23*) CCP/C ratios due to unreliably detected concentrations of citrate. However, we included only metabolites and resulting ratios with sufficient concentration, because %SD depends on metabolite concentration (*19*); therefore, we may have potentially excluded some voxels with low concentrations of metabolites. In several sextants, we were unable to detect good-quality voxels, significantly decreasing the reliability of cancer detection. As previously stated, all ^{1}H-MRS data in our study were obtained without an endorectal coil. In addition to dramatically increased patient comfort, the protocol we applied also allowed for the use of the obtained anatomic MRI information in radiotherapy planning, because deformation of local prostate anatomy caused by endorectal coils is avoided (*24*).

Visual analysis of contrast-enhanced MRI and PET/CT had the same agreement with cancer laterality based on biopsy results: 71%. Nevertheless, some tumor lesions were detected solely by ^{11}C-acetate PET/CT and ^{1}H-MRS (Fig. 4). In a similar study (*25*) in which laterality of the primary prostate cancer lesion was determined by single-voxel ^{1}H-MRS and SUV maximum of ^{11}C-choline PET, the agreement with pathology findings was 50% on ^{1}H-MRS and 81% on PET. However, this study by Yamaguchi et al. (*25*) was limited by the lack of exact anatomic localization of observed ^{11}C-choline uptake, because of missing image fusion with CT or MRI. Moreover, single-voxel ^{1}H-MRS, covering partly 1 lobe of the prostate gland at a time, was performed in contrast to multivoxel ^{1}H-MRS, which covers the entire prostate gland in a single scan in the current study. The major limitation of our study, in turn, is the small number of patients (38%) with detailed histologic information from prostatectomy specimens.

Detection of cancer and the dominant lobe based on visual analysis alone was better than quantitative interpretation (SUV) of ^{11}C-acetate PET/CT data. The superiority of visual interpretation may be due to the shape and presentation of ^{11}C-acetate hot spots, which, in the case of cancer, tend to be more distinct and to localize in the peripheral region, as opposed to the more diffuse and symmetric centralized uptake in the case of hyperplasia. This difference in uptake pattern demonstrates the limitations of the sole use of SUV in clinical decision making and stresses the need for a highly experienced ^{11}C-acetate PET reader.

CONCLUSION

Our study indicates that quantitative analysis of prostate cancer metabolism with ^{11}C-acetate PET and ^{1}H-MRS does not correlate with prostate cancer aggressiveness. ^{11}C-acetate PET/CT and MRI detect prostate cancer laterality with com-

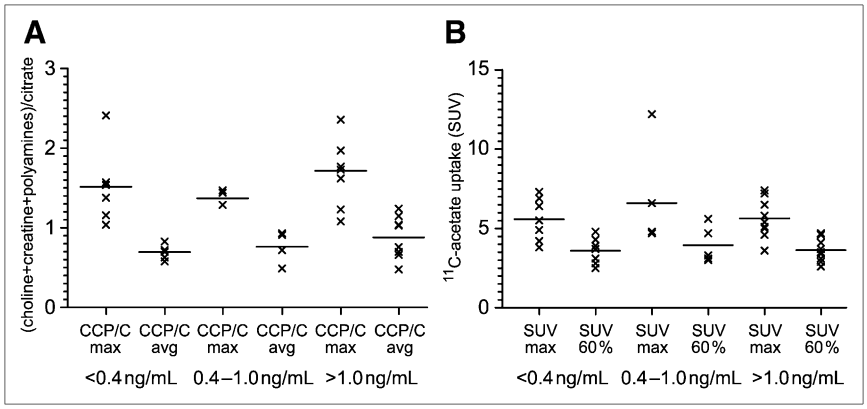

FIGURE 3. Quantitative ^{1}H-MRS (A) and ^{11}C acetate PET/CT (B) show no difference between patients with low (<0.4 ng/mL/y), intermediate (0.4–1.0 ng/mL/y), or high (>1.0 ng/mL/y) PSA velocity. avg = average; max = maximum.

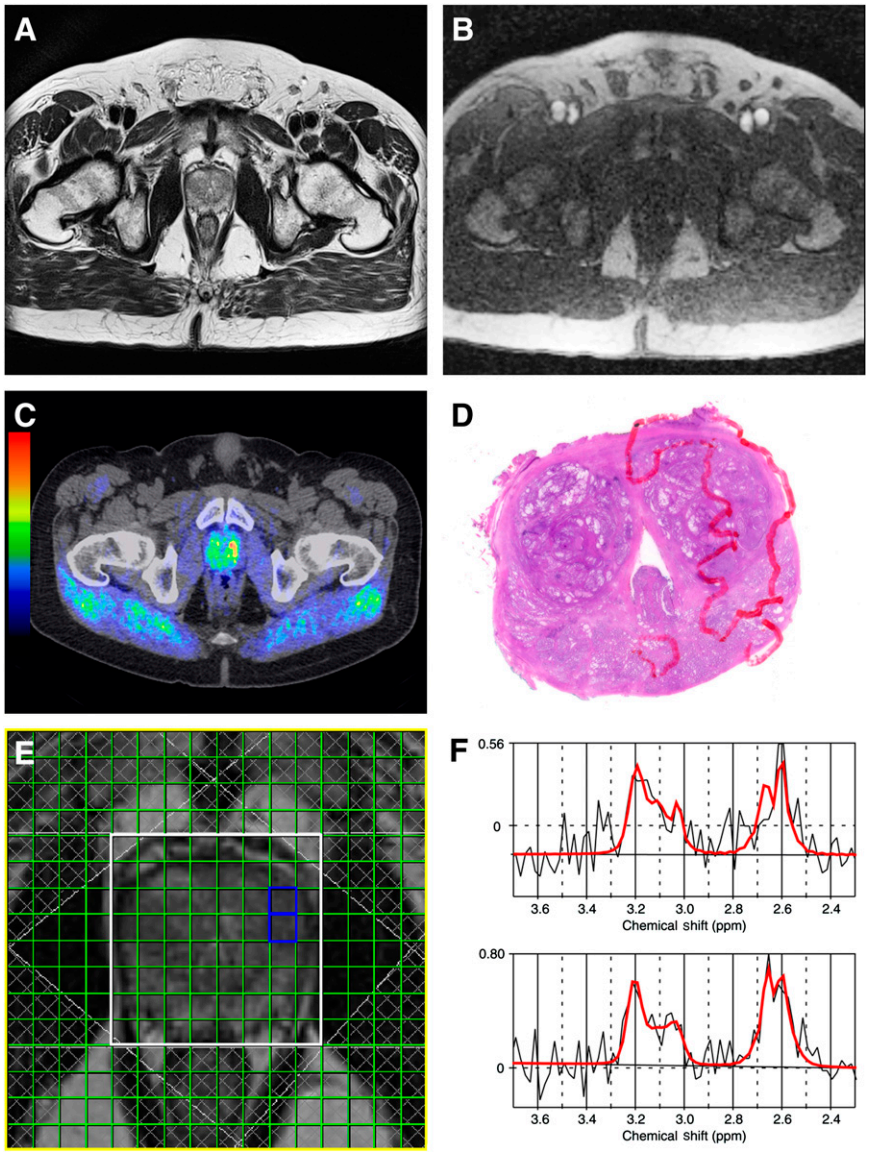

FIGURE 4. T2-weighted MR image (A), contrast-enhanced MR image (B), ^{11}C-acetate PET/CT image (C), most closely correlated histologic slice (D), and T2-weighted MRI slice (E) showing 2 voxels with corresponding spectra (F) of patient 8 with adenocarcinoma (Gleason score, 3 + 4) in left prostatic lobe. Signal intensity and contrast enhancement are not decreased in A and B, respectively. C is scaled to SUV, with a minimum at 0.95 and maximum at 6.37. Areas of cancer are marked with red ink on histologic macroslice (D). Spectra (F) from involved areas depicted in E show high CCP/C ratios of 1.258 and 0.978, which are characteristic of cancer. ppm = parts per million.

parable but limited accuracy. Finally, our study does not lend support to the use of ^{11}C-acetate PET/CT in the primary diagnosis of prostate cancer suspected on PSA screening.

ACKNOWLEDGMENTS

We thank the staff of Turku PET Centre and the Department of Diagnostic Radiology, University of Turku, for their continued support; Irina Lisinen for help with statistical analysis; and, especially, Prof. Peter B. Dean for reviewing the manuscript. Financial support has been provided by the Finnish Cancer Organisations and Sigrid Jusélius Foundation and through the Turku University Hospital EVO funding.

REFERENCES

1. Dennis LK, Resnick MI. Analysis of recent trends in prostate cancer incidence and mortality. *Prostate.* 2000;42:247–252.
2. Presti JC Jr, Hricak H, Narayan PA, Shinohara K, White S, Carroll PR. Local staging of prostatic carcinoma: comparison of transrectal sonography and endorectal MR imaging. *AJR.* 1996;166:103–108.
3. Weinreb JC, Blume JD, Coakley FV, et al. Prostate cancer: sextant localization at MR imaging and MR spectroscopic imaging before prostatectomy—results of ACRIN prospective multi-institutional clinicopathologic study. *Radiology.* 2009;251:122–133.
4. Vilanova JC, Comet J, Barcelo-Vidal C, et al. Peripheral zone prostate cancer in patients with elevated PSA levels and low free-to-total PSA ratio: detection with MR imaging and MR spectroscopy. *Radiology.* 2009;253:135–143.
5. Costouros NG, Coakley FV, Westphalen AC, et al. Diagnosis of prostate cancer in patients with an elevated prostate-specific antigen level: role of endorectal MRI and MR spectroscopic imaging. *AJR.* 2007;188:812–816.
6. Hricak H, Choyke PL, Eberhardt SC, Leibel SA, Scardino PT. Imaging prostate cancer: a multidisciplinary perspective. *Radiology.* 2007;243:28–53.
7. Liu IJ, Zafar MB, Lai YH, Segall GM, Terris MK. Fluorodeoxyglucose positron emission tomography studies in diagnosis and staging of clinically organ-confined prostate cancer. *Urology.* 2001;57:108–111.
8. Sandblom G, Sorensen J, Lundin N, Haggman M, Malmstrom PU. Positron emission tomography with ^{11}C-acetate for tumor detection and localization in patients with prostate-specific antigen relapse after radical prostatectomy. *Urology.* 2006;67:996–1000.
9. Oyama N, Miller TR, Dehdashti F, et al. ^{11}C-acetate PET imaging of prostate cancer: detection of recurrent disease at PSA relapse. *J Nucl Med.* 2003;44:549–555.

10. Wachter S, Tomek S, Kurtaran A, et al. ^{11}C-acetate positron emission tomography imaging and image fusion with computed tomography and magnetic resonance imaging in patients with recurrent prostate cancer. *J Clin Oncol.* 2006;24:2513–2519.
11. Kotzerke J, Volkmer BG, Glatting G, et al. Intraindividual comparison of [^{11}C] acetate and [^{11}C]choline PET for detection of metastases of prostate cancer. *Nuklearmedizin.* 2003;42:25–30.
12. Kelloff GJ, Choyke P, Coffey DS. Challenges in clinical prostate cancer: role of imaging. *AJR.* 2009;192:1455–1470.
13. Morris MJ, Scher HI. ^{11}C-acetate PET imaging in prostate cancer. *Eur J Nucl Med Mol Imaging.* 2007;34:181–184.
14. Vavere AL, Kridel SJ, Wheeler FB, Lewis JS. 1-^{11}C-acetate as a PET radiopharmaceutical for imaging fatty acid synthase expression in prostate cancer. *J Nucl Med.* 2008;49:327–334.
15. Yoshimoto M, Waki A, Yonekura Y, et al. Characterization of acetate metabolism in tumor cells in relation to cell proliferation: acetate metabolism in tumor cells. *Nucl Med Biol.* 2001;28:117–122.
16. Pike VW, Eakins MN, Allan RM, Selwyn AP. Preparation of [1-^{11}C]acetate: an agent for the study of myocardial metabolism by positron emission tomography. *Int J Appl Radiat Isot.* 1982;33:505–512.
17. Seppala J, Seppanen M, Arponen E, Lindholm P, Minn H. Carbon-11 acetate PET/CT based dose escalated IMRT in prostate cancer. *Radiother Oncol.* 2009;93:234–240.
18. Kato T, Tsukamoto E, Kuge Y, et al. Accumulation of [^{11}C]acetate in normal prostate and benign prostatic hyperplasia: comparison with prostate cancer. *Eur J Nucl Med Mol Imaging.* 2002;29:1492–1495.
19. Provencher SW. Estimation of metabolite concentrations from localized in vivo proton NMR spectra. *Magn Reson Med.* 1993;30:672–679.
20. Mazaheri Y, Shukla-Dave A, Hricak H, et al. Prostate cancer: identification with combined diffusion-weighted MR imaging and 3D ^{1}H MR spectroscopic imaging—correlation with pathologic findings. *Radiology.* 2008;246:480–488.
21. Ahmed HU. The index lesion and the origin of prostate cancer. *N Engl J Med.* 2009;361:1704–1706.
22. Oyama N, Akino H, Kanamaru H, et al. ^{11}C-acetate PET imaging of prostate cancer. *J Nucl Med.* 2002;43:181–186.
23. Reinsberg SA, Payne GS, Riches SF, et al. Combined use of diffusion-weighted MRI and ^{1}H MR spectroscopy to increase accuracy in prostate cancer detection. *AJR.* 2007;188:91–98.
24. Heijmink SW, Scheenen TW, van Lin EN, et al. Changes in prostate shape and volume and their implications for radiotherapy after introduction of endorectal balloon as determined by MRI at 3T. *Int J Radiat Oncol Biol Phys.* 2009;73:1446–1453.
25. Yamaguchi T, Lee J, Uemura H, et al. Prostate cancer: a comparative study of ^{11}C-choline PET and MR imaging combined with proton MR spectroscopy. *Eur J Nucl Med Mol Imaging.* 2005;32:742–748.